ELSEVIER

Materials Science and Engineering A325 (2002) 511–519

MATERIALS SCIENCE & ENGINEERING A

www.elsevier.com/locate/msea

Stacking fault energy in short-range ordered γ-phases of Ni-based superalloys

F. Pettinari [a], J. Douin [b], G. Saada [b], P. Caron [c], A. Coujou [a], N. Clément [a,*]

[a] *CEMES/CNRS, 29 rue Jeanne Marvig, BP 4347, 31055 Toulouse Cedex, France*
[b] *LEM-CNRS/ONERA, 29 avenue de la Division Leclerc, BP 72, 92322 Châtillon Cedex, France*
[c] *DMMP, ONERA, 29 avenue de la Division Leclerc, BP 72, 92322 Châtillon Cedex, France*

Received 27 December 2000; received in revised form 23 July 2001

Abstract

Several aspects on the stacking fault energy (SFE) in short-range ordered γ-phase model alloys of new nickel based superalloys are discussed. Using transmission electron microscope weak beam observations and computer simulated images of dissociation widths, the SFE was determined as a function of temperature. The values for both alloys are close (31 ± 4 mJ m^{-2} for the Re-containing alloy and 28 ± 6 mJ m^{-2} for the Ru-containing alloy). In both cases, the dissociation widths remain quite constant up to 350 °C and a slight decrease is observed at higher temperature. The deformation micromechanisms and the constancy of the SFE up to 750 °C are analysed in connection with short-range order. The deformation at low temperature is characterised by dislocation pile ups, the influence on the dissociation widths of the internal stress due to such configuration is analysed. The calculation reveals a strong effect on the leading dislocation of the pile-up whose dissociation distance can be reduced at most by 50%.

Keywords: Stacking fault energy; Deformation mechanisms; Short range ordered solid solutions; Dislocation pile-up

1. Introduction

Ni-based single-crystal superalloys are currently being developed for gas turbine blade and vane applications. These alloys are especially designed to obtain a high creep and fatigue strength at elevated temperature, together with a good hot corrosion and oxidation resistance [1]. They are constituted by a face centred cubic austenitic γ matrix strengthened by a high volume fraction (up to 70%) of finely dispersed ordered γ′ ($L1_2$) precipitates. Besides, these materials contain a number of alloying elements (between 8 and 10), each of them having a specific role in the mechanical and environmental properties. Among these elements, rhenium was added in the second and third generation of single-crystal superalloys [2,3], while ruthenium was more recently introduced in some new-generation alloys developed at ONERA [4,5].

The complex f.c.c. γ solid solution contains a large amount of Cr along with elements such as Mo, Co, some refractory elements (W, Re or Ru) which go preferentially to the γ-matrix [6,7], as well as some γ′-forming elements such as Al, Ti and Ta [8]. The γ phase is also characterised by the presence of short-range order (SRO) and/or $L1_2$-type long-range order [9–11]. The presence of SRO, which induces a local shear resistance higher than the critical resolved shear stress [12], is associated with an improvement of the mechanical properties at low temperature [11].

In these alloys, the $a/2\langle 110\rangle$ dislocations are usually dissociated into two $a/6\langle 112\rangle$ partial dislocations with a stacking fault in between, according to, for example:

$$\frac{a}{2}[\bar{1}01] \rightarrow \frac{a}{6}[\bar{2}11] + \mathrm{SF} + \frac{a}{6}[\bar{1}\bar{1}2] \quad (1)$$

in the (111) plane. The SFE in such complex γ phases of industrial alloys is an important microscopic parameter that directly influences the different properties and propagation modes of dislocations, for exam-

* Corresponding author. Tel.: +33-5-62-257873; fax: +33-5-62-257999.
E-mail address: clement@cemes.fr (N. Clément).

0921-5093/02/$ - see front matter
PII: S0921-5093(01)01765-8

ple the dislocation flexibility when they enter the γ channels, the cross slip of screw segments, the dislocation climb of edge dislocations along the interfaces, the shearing of γ′ particles [13]. This parameter, evaluated by many authors, varies as a function of the nature and concentration of the constituents. In binary Ni–Cr solid solutions the addition of 10% of Co makes the SFE drop from 75 to 56 mJ m^{-2} [14,15]. The addition of supplementary elements such as Ti, Al, Ta, Mo and W that are present in the γ phases of industrial superalloys, results in a decrease of the SFE down to 20–30 mJ m^{-2} [13]. Up to now, the influence on the SFE of Re or Ru is not known.

The purpose of this work is to evaluate the SFEs values in short range ordered γ phase model alloys when the deformation temperature varies and to determine the controlling deformation parameters. As the deformation in this category of alloys proceeds mainly through the propagation of dislocation pile ups, the influence of the internal stress due to this dislocation distribution on the dissociation distances is also analysed.

2. Experimental

The alloys investigated here are single phases γ alloys whose simplified chemical compositions ('model alloys') were derived from that of the γ phases of industrial single crystal superalloys. They contain, respectively, some Re and some Ru and will be referred to in the following as γ_{MCRe} and γ_{MCRu}. In order to avoid some undesirable long range order effects, nickel was substituted for γ′-formers elements (Al, Ti, Ta). The corresponding chemical compositions (reported in Table 1) are, therefore, limited to five elements.

Table 1
Chemical composition of the alloys under study (in at.%)

	Ni	Cr	Mo	W	Re	Ru
γ_{MCRe}	65.60	26.21	2.02	1.98	4.19	–
γ_{MCRu}	65.88	26.07	2.03	1.98	–	4.04

Table 2
Numerical values for the elastic constants C_{11}, C_{12}, and C_{44} from [18]

T	25 °C	350 °C	750 °C	1050 °C
C_{11} (GPa)	242	232	210	192
C_{12} (GPa)	153	148	142	138
C_{44} (GPa)	128	118	101	90

Master heats of both alloys were melted in a high vacuum induction furnace. Single crystals rods of these alloys were then grown by the withdrawal process using pre-oriented ⟨001⟩ seeds. They were then subjected to a heat treatment at 1330 °C for 100 h followed by air cooling, in order to homogenise the chemical segregation resulting from the directional solidification. Cylindrical specimens (gauge length = 30 mm and diameter = 4 mm) machined from the heat treated single crystal bars with ⟨001⟩ orientation were deformed in tension ($\dot{\varepsilon} \cong 10^{-4}\ s^{-1}$) between 1.5 and 2% of plastic strain at 25, 350, 750 and 1050 °C, then air cooled. Microsamples were cut from deformed ⟨001⟩ single crystal tensile specimens. For such an orientation multiple slip is operative.

Thin slices parallel to {111} slip bands, thinned down by electropolishing, were observed in a JEOL 200CX Transmission Electron Microscope (TEM) using an operating voltage of 200 kV or in a High Voltage Electron Microscope (HVEM-CEMES/Toulouse) with an operating voltage of 2 MV. The determination of the dissociation widths was carried out with the JEOL 200CX, in as close as possible weak-beam conditions with **g**–2**g** or **g**–3**g** diffracting conditions and $|\mathbf{g}\mathbf{b}_t| = 2$($\mathbf{b}_t$; Burgers vector of the total dislocation). Notice that, as the contrast of dislocations is rather low in such Ni–Cr solid solutions, the chosen value of the deviation parameter s_g (deviation from Bragg angle: $|s_g| \sim 0.2\ nm^{-1}$) corresponds to a compromise between the better weak-beam conditions and a sufficient contrast of the images.

The observed distances between the intensity peaks on TEM micrographs were measured using a magnification $G \cong 250{,}000$. This allows an accuracy of ± 0.4 nm while the uncertainty on the dislocation character was estimated as less than 5°. With such a s_g value, the splitting widths values can be evaluated with an accuracy better than 10%.

Experimentally, the dissociation widths directly measured from TEM images differ from the real values [16]. In order to evaluate precisely the SFEs, the dissociation widths between the two partial dislocations, corrected for the inclination of the dissociation plane, were measured and compared with simulated images computed using the CUFOUR many beam image simulation program of Schäublin and Stadelmann [17]. For the calculations, the acceleration voltage was taken to be 200 kV and the thickness foil was 200 nm. It has been assumed that the solid solutions are close to Ni_3Cr, the atoms being considered as arranged in a disordered solid solution. The images were calculated using a diffraction vector **g** of the ⟨220⟩-type in **g**–2**g** or **g**–3**g** diffracting conditions. The elastic constants C_{11}, C_{12} and C_{44} used were the ones evaluated at different temperatures in the γ-matrix of the CMSX-3 nickel base superalloy [18] (see Table 2).

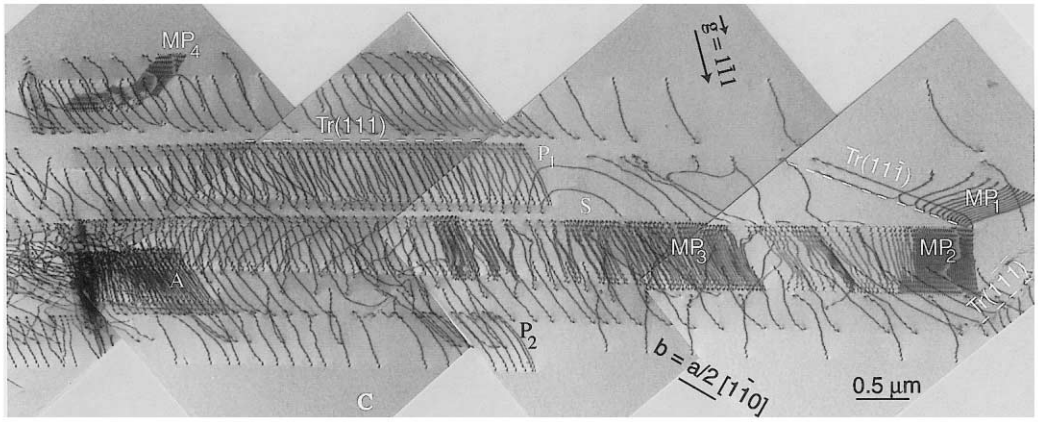

Fig. 1. General aspect of the microstructure at $T < 750$ °C in γ_{MCRe}. Diffracting vector $\mathbf{g} = 1\bar{1}1$. The presence of a localised slip band is shown here: within the slip band, a dislocation source is visible in S, and neighbouring pile ups are observed to reorganise in multipoles (MP). The operating voltage is 200 kV.

3. Stacking fault energy γ_{SF} and deformation mechanisms

3.1. Particular deformation aspects of short range ordered solid solutions

As the aim of this study is to define the parameters that control the deformation of the investigated solid solutions, the characteristics of the deformation microstructure are first presented followed by SFE measurements.

Typical microstructures of samples deformed at 350 and 1050 °C are shown in Figs. 1 and 2. The thin foils were cut parallel to {111} slip traces left on the sample by the macroscopic deformation ($\cong 2\%$). The micrographs were taken at room temperature, under bright field conditions.

Some traces of the glide planes (intersection between the glide plane and the foil plane) are visible in γ_{MCRe} after deformation at 350 °C (Fig. 1). They allow to characterise the different active glide planes: the (111) and (11$\bar{1}$) planes are inclined with respect of the thin foil plane while the (1$\bar{1}\bar{1}$) plane is seen edge on. Severely work-hardened areas are visible (*A*). They consist essentially in numerous planar pile-ups of several tens of dislocations, which most often are stopped in the middle of the foil without any apparent obstacle, indicating a high local friction stress. The curvature of the dislocation *S* suggests the presence of a dislocation source at the origin of pile-ups before the thin foil preparation. Numerous dipoles and multipoles (noted MP) are visible. Non deformed zones exist also in these images (*C*). Thus, the dislocations sources seem to be distributed heterogeneously in the sample so that deformation extends from these zones by creating bundles of slip lines. Dipoles and multipoles result from the interactions between different moving dislocations groups of opposite Burgers vectors, gliding on close parallel planes. Their presence is characteristic of planar movements [19]. We have observed such a localised deformation at every temperature between 25 and 750 °C, in γ_{MCRe} and γ_{MCRu}. Notice that in this temperature range, only a very small number of extended stacking faults is observed.

At the heads of the pile-ups, the two leading dislocations appear to be paired (for example see P_1 and P_2 in Fig. 1) since, during in situ deformation experiments, the movements of these two dislocations are correlated [12]. This pairing is found in samples deformed from room temperature and up to 750 °C, but it is not observed anymore beyond 750 °C. At 1050 °C, individual movements of dislocations exist and the deformation is homogeneous (Fig. 2). The individual dislocations distributed now homogeneously in the thin foil may take the form of small closed loops (A) or wide open loops (B). The presence of both loops and tangles indicates that cross slip associated with climb operates at this temperature.

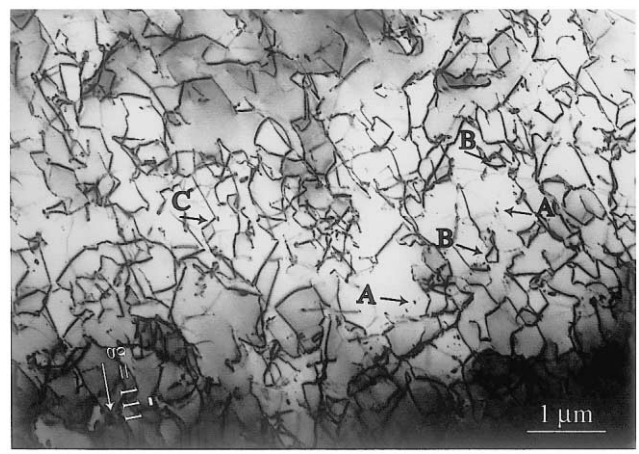

Fig. 2. $T = 1050$ °C in γ_{MCRe}. $\mathbf{g} = 1\bar{1}1$. Deformation is homogeneously distributed. Small closed loops are visible in A, open loops in B. The operating voltage is 2 MeV.

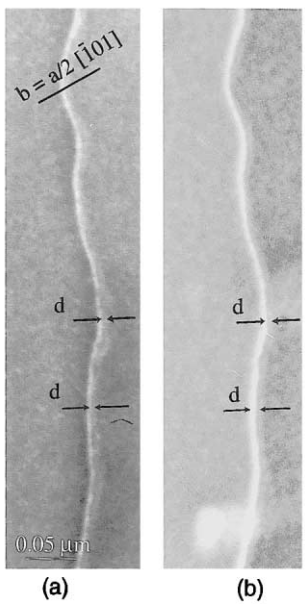

Fig. 3. In situ heating experiment of an isolated dislocation: weak beam conditions $\mathbf{g}-2\mathbf{g}$, $\mathbf{g}=\overline{2}\overline{2}0$, $\mathbf{gb}=2$; (a) γ_{MCRu}, $T=25$ °C, dissociation width: 6.8 nm $< d <$ 7.6 nm; (b) γ_{MCRu}, $T=350$ °C, same dislocation, same dissociation width, 6.7 nm $< d <$ 7.5 nm.

3.2. Splitting widths determination

In the following observations, the separation distances measured in the TEM at 20 °C are supposed to be identical to those existing during deformation at higher temperatures. The validity of such hypothesis was confirmed during an in-situ experiment, by measuring the dissociation distance on the same dislocation, first at room temperature then at 350 °C, during in-situ heating of the sample in the TEM. The corresponding images are given in Fig. 3. The dissociation width is observed to remain constant within experimental errors: $d=7.2\pm0.4$ nm at 25 °C, and $d=7.2\pm0.3$ nm at 350 °C for a character $\Phi=65°$. Thus, between room temperature and 350 °C the measured 'in situ' and 'post mortem' dissociation between partials give the same result. As, above 750 °C, measurements done at room temperature show a slight decrease of the splitting width, we can conclude that the dissociation is not too much disturbed by cooling.

In order to determine as precisely as possible the SFEs, the dissociation width were measured and compared with simulated images. A simulated image with its intensity profile is illustrated in Fig. 4. It corresponds to the experimental dissociation of a dislocation, found in a γ_{MCRe} sample deformed at 350 °C, illustrated in A in Fig. 5a. In the present case, the dissociation width measured in the TEM image (6.8 ± 0.7 nm) corresponds to a real distance between dislocations of 7.5 nm for a character $\phi=68°$. In our case where s_g is about 0.2 nm^{-1} we have checked that the difference between observed and real widths is small, in the order or less than of the error made during measurements.

Stacking faults measurements were done on dislocations belonging to pile ups and situated within these pile ups (the two head dislocations which are paired [12] being always excluded). The term 'isolated' used in the following concerns dislocations far from their neighbours and in most cases located at the tail of the pile ups. In such cases, as in these planes, whatever the temperature, SRO is destroyed by the first pair, friction forces are weak [12] and an actual stacking fault energy can be measured.

The dislocation in Fig. 5a is curved enough to allow the study of the influence of the character ϕ on the dissociation distance d. Notice that at this temperature, some pinching or pinning probably due to chemical heterogeneities are visible on partial dislocations (see C and D Fig. 5a). The measurements of d(ϕ) are shown

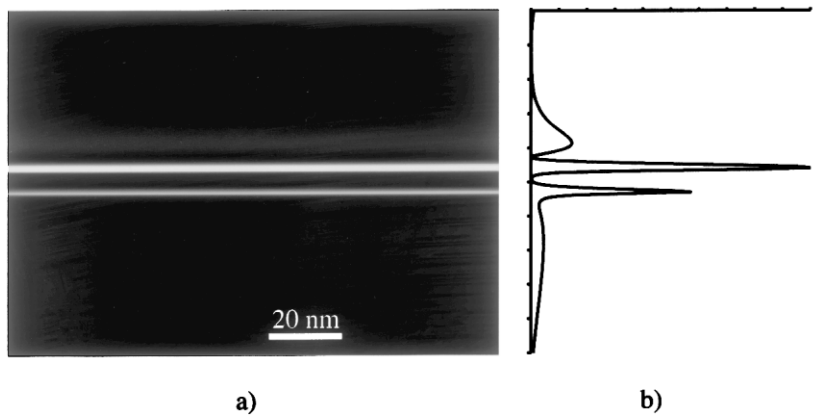

Fig. 4. (a) Computer simulated image of the dislocation dissociation in γ_{MCRe} deformed at 350 °C illustrated in A Fig. 5a, using CUFOUR Program; (b) Intensity profile. Simulation parameters; Acceleration voltage 200 kV, foil thickness 200 nm, diffraction vector $\mathbf{g}=\overline{2}02$ in $\mathbf{g}-3.2\mathbf{g}$ diffracting conditions, beam direction 111, elastic constants C_{11}, C_{12} and C_{44} from [18]; Burgers vectors $b=a/2[\overline{1}01]$ dissociated according to Eq. (1); line direction character $[1\overline{6}5]$ ($\phi=68°$); real dissociation distance $d_s=7.5$ nm.

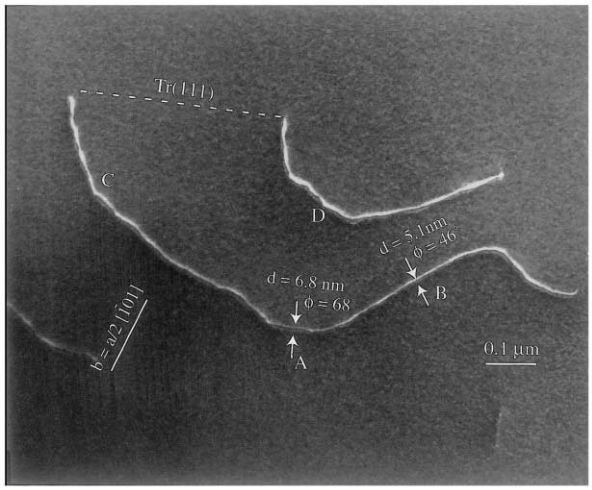

(a)

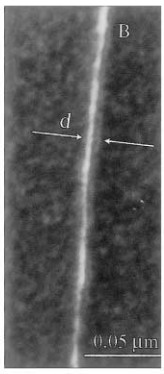

(b)

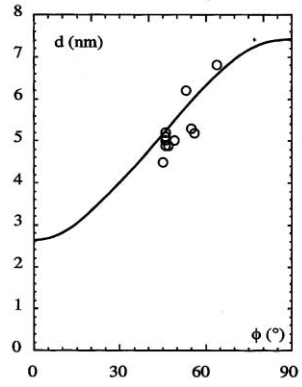

(c)

Fig. 5. Dissociation of dislocations in γ_{MCRe}; (a) $T = 350$ °C; weak beam conditions $\mathbf{g}-3\mathbf{g}$, $\mathbf{g} = 20\bar{2}$, $\mathbf{gb} = 2$, A and B: examples of dissociation (A: $d = 6.8 \pm 0.7$ nm for a character $\Phi = 68°$, and B: $d = 5.1 \pm 0.5$ nm for a character $\Phi = 46°$, C and D: anchoring points; (b) enlargement of area B; (c) Comparison between the theoretical variation of the dissociation distance d as a function of the character ϕ, as predicted by anisotropic elasticity using DISDI program, for $\gamma_{SF} = 31$ mJ m^{-2} (solid line) and experimental points.

in Fig. 5c. The determination of the SFE can then be made in the framework of anisotropic elasticity using the DISDI program of Douin [20]. For this calculation, the lattice parameter of the investigated f.c.c. structure was $a = 0.358$ nm, the elastic constants taken were from [18], the anisotropy factor in these alloys being about 3. The experimental dissociation distances after deformation at 350 °C fit rather well with the theoretical curve obtained for the SFE: $\gamma_{SF} = 31 \pm 3$ mJ m^{-2} (Fig. 5c).

Another case of dissociation of a dislocation observed in the γ_{MCRu}, deformed at 750 °C is presented in Fig. 6. The dissociation width between the two partials is 7.2 ± 0.7 nm for a character $\phi = 82°$ and 6.8 ± 0.7 nm for $\phi = 77°$, leading to the SFE: $\gamma_{SF} = 26 \pm 3$ mJ m^{-2}. We have also checked that these experimental values fit rather well with the theoretical curve obtained assuming anisotropic elasticity.

The determinations of the SFE for both alloys, from 25 to 1050 °C, are listed in Table 3 as well as the dissociation widths obtained for a dissociated $1/2\langle 110\rangle$ 60° mixed dislocation. They both appear to be rather stable (for γ_{MCRe}, $\gamma_{SF} = 30 \pm 3$ mJ m^{-2} and γ_{MCRu}, $\gamma_{SF} = 27 \pm 4$ mJ m^{-2}). Around 750 °C, a small but noticeable decrease can be mentioned.

3.3. Dissociation width within the dislocation pile up

As the movement of dislocation pile ups controls the deformation and in order to evaluate the pile up effect, if any, on the dissociation width, measurements were systematically done on all the dislocations belonging to the same pile up, for example, in γ_{MCRu} deformed at 25 °C (Fig. 7). The dissociation into two partial dislocations of each dislocation is clearly visible and measurable. All dislocations are oriented close to the edge character ($\phi = 75°$). A particularly strong contrast usually appears on the first dislocation of the pile ups (denoted by 1), which disturbs the determination of the corresponding dissociation. For the others dislocations, the observed value $d = 8 \pm 0.8$ nm for $\phi = 75°$ which is quite similar to the value measured on 'isolated' dislocations situated far away from others within the pile up and not disturbed by their elastic interaction. In a same pile up, the dissociation width does not depend on the dislocation position and thus remains quite constant all along the pile-up.

The pile up effect has been analysed in the particular case of the head dislocation. Assuming that the leading partial of this head perfect dislocation is locked by the SRO, the equilibrium of the corresponding trailing partial can be written as:

$$F_{2\text{-}1}(d') = \gamma + F_{2\text{-pu}} \tag{2}$$

where F_{2-1} is the repulsive interaction force between partials 1 and 2 at a distance d', and F_{2-pu} is the resultant of the interaction forces between partial 2 and the dislocations of the pile-up (Fig. 8). In order to simplify the calculations, we consider that the pile up is constituted of perfect dislocations (except of course the leading one which is dissociated) and that its dissociation width does not influence noticeably the distance between perfect dislocations. The force F_{2-pu} acting per unit length on the partial dislocation 2 created by n perfect $a/2[\bar{1}01]$ dislocations, as a function of the character ϕ of the perfect dislocations, is:

$$F_{2\text{-pu}} = \sum_{j=1,n} \frac{\mu a^2(6 - 3\nu - 3\nu\cos 2\phi + \varepsilon\sqrt{3}\sin 2\phi)}{48\pi(1-\nu)r_{2j}} \tag{3}$$

where ε is $+1$ if the trailing partial dislocation has a Burgers vector $a/6[\bar{2}11]$ and -1 for a Burgers vector $a/6[\bar{1}\bar{1}2]$; μ is the shear modulus and ν the Poisson ratio; r_{2j} are the distances (determined experimentally)

between the partial dislocation 2 and the perfect dislocations j (Fig. 8b).

As F_{2-pu} is not a function of the equilibrium distance d', everything happens as if the SFE was locally changed by the presence of the pile up from γ to $(\gamma + \Delta\gamma)$ with $\Delta\gamma = F_{2-pu}$. The evaluation of the interaction forces was carried out in the example of the pile-up in Fig. 7: the perfect dislocations are distant, respectively, from 30, 90 then 140 nm, and for any other dislocation, the distance is about 140 nm. For our calculations, ten perfect dislocations have been included, but we have verified, and it was very predictable, that only the nearest ones have a significant influence. The calculated value of the variation $\Delta\gamma = F_{2-pu}$ and the corresponding equilibrium distance as a function of ϕ are illustrated in Fig. 9. The maximum force corresponds to an increase in the order of the surface tension γ_{SF} ($\cong 30$ mJ m^{-2}). This means that, due to the stress concentration created by the pile up, the dissociation width of the head dislocation can roughly decrease up to 50%.

Notice that the theoretical mean stress on a dislocation in the middle of an infinite pile up at equilibrium is zero, and we have also verified that for a dislocation within an even small finite pile up the related variation of dissociation distance is very low and should not be detectable. In agreement, the dissociation distance d measured inside the pile-up appears to be constant within the experimental scattering.

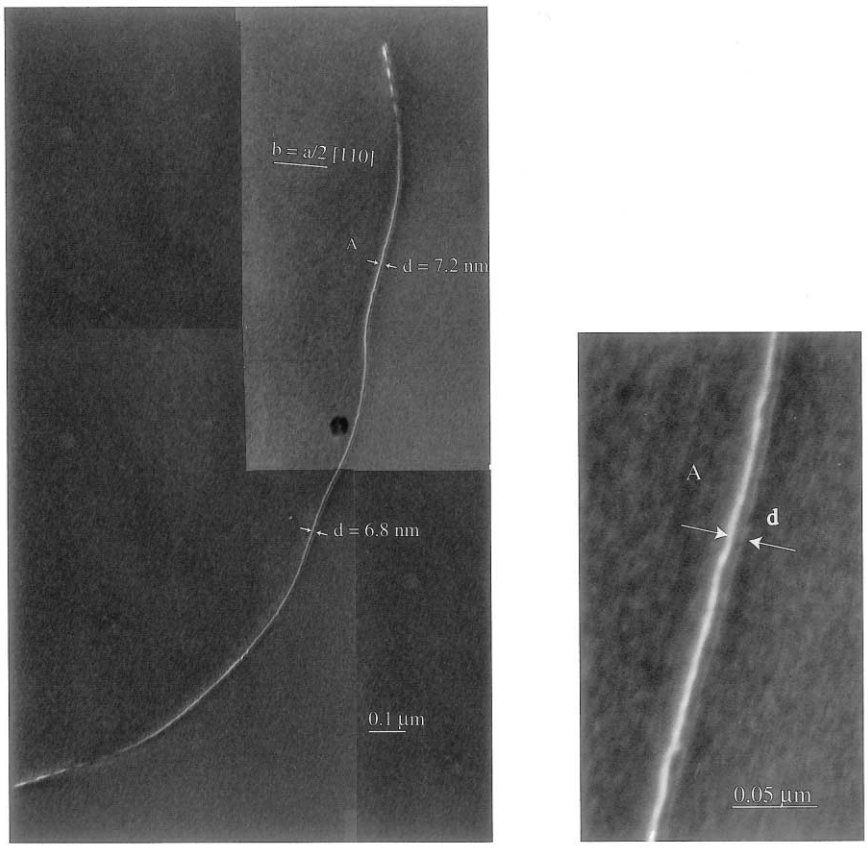

Fig. 6. Dissociation of an 'isolated' dislocation in γ_{MCRu}; (a) $T = 750$ °C, weak beam conditions $\mathbf{g}$–$3\mathbf{g}$, $\mathbf{g} = 2\bar{2}0$, $\mathbf{gb} = 2$; (b) enlargement of area A ($d = 7.2 \pm 0.7$ nm for $\Phi = 82°$).

Table 3
Dissociation width (d) for 60° mixed dislocations and stacking fault energy (γ_{SF}) as a function of temperature in γ_{MCRe} and γ_{MCRu}

	T = 25 °C		$T = 350$ °C		$T = 750$ °C		$T = 1050$ °C	
	γ_{MCRe}	γ_{MCRu}	γ_{MCRe}	γ_{MCRu}	γ_{MCRe}	γ_{MCRu}	γ_{MCRe}	γ_{MCRu}
d (nm)	6.7 ± 0.7	6.7 ± 0.7	6.4 ± 0.6	6.9 ± 0.7	5.7 ± 0.6	6.4 ± 0.7	5.7 ± 0.6	5.9 ± 0.6
γ_{SF} (mJ m-2)	32 ± 3	31 ± 3	31 ± 3	28 ± 2	30 ± 3	26 ± 3	27 ± 3	25 ± 3

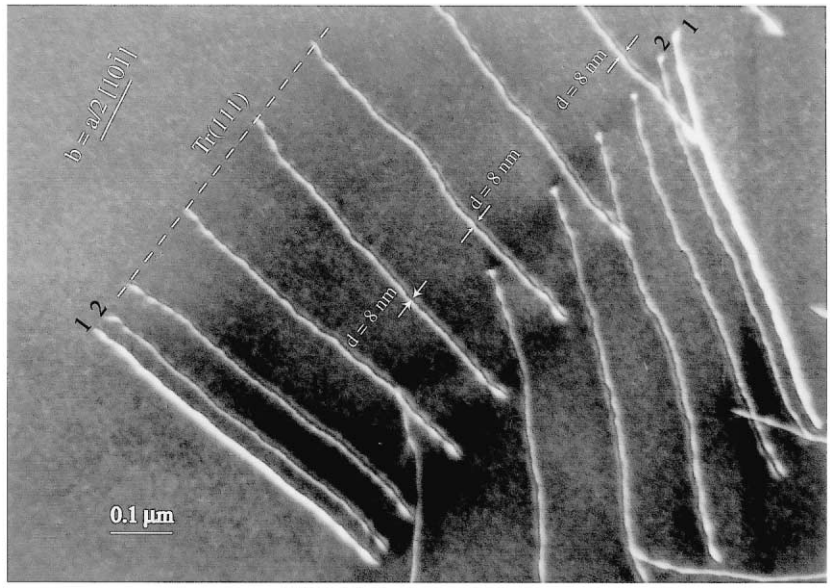

Fig. 7. Dissociation of dislocations within a pile up in γ_{MCRu} deformed at $T = 25$ °C, weak beam conditions $\mathbf{g}$–$3\mathbf{g}$, $\mathbf{g} = \bar{2}02$, $\mathbf{gb} = 2$. Head dislocations (1 and 2) appear to be paired and a strong particular contrast is visible on 1. In the rest of the pile up the dissociation width remains quite constant $d = 8 \pm 0.8$ nm ($\Phi = 75°$).

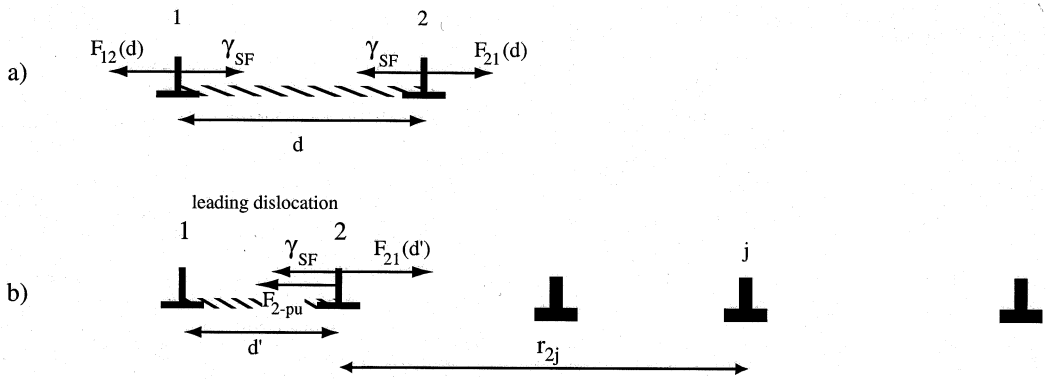

Fig. 8. Effect of the pile-up on the dissociation width. (a) Equilibrium of one isolated dissociated dislocation. $F_{21}(d)$ corresponds to the elastic interaction at a distance d, γ_{SF} is the stacking fault energy; (b) Equilibrium of the same dislocation at the head of a pile-up assuming that partial 1 is locked. F_{2-pu} is the resultant on the partial 2 of the forces due to the presence of the pile up. The dissociation distance is now d' ($d' \neq d$); the difference between d and d' depends on the sign of $\Delta\gamma = F_{2-pu}$. In the illustrated configuration, $\Delta\gamma > 0$ then $d' < d$.

3.4. Special contrast for the dislocation at the head of the pile up

As indicated above, the dislocations at the head of the pile up consistently show a different contrast from the other dislocations within the pile up (see dislocations noted 1 in Fig. 7 for example). We have first verified that taking into account only a decrease of the dissociation width does not explain this contrast change. A change of contrast could reflect a local modification of the displacement field around the dislocation coming from the SRO. However, if there was such an effect resulting from the SRO, it should not only be visible on the leading dislocation of the pile ups but also on dislocations not belonging to a pile up. This has not been evidenced. Finally, as the relative intensity of the contrast of the leading dislocation changes with the sign of $\mathbf{g}$, it is believed than this effect is coming from an effect of different imaging conditions for this dislocation, resulting from the presence of the pile up.

The stress field generated by an infinite pile up is zero everywhere but not at the head of the pile up, thus only the head dislocation can undergo a change in contrast if any. This can be exemplified by calculating the local elastic rotation tensor π_{ij} at the head of a pile up of pure edge dislocations. Assuming elastic isotropy, one finds for one edge dislocation that the only non-zero component is the rotation of the crystal around the direction of the dislocations, with an amplitude ω_3:

$$\omega_3 = -\frac{b\cos\theta}{2\pi r} \quad (4)$$

where b is the modulus of the edge dislocation and r and θ the cylindrical coordinates related to the dislocation. As an approximation, assuming a pile up of 10–40 gives a rotation angle of the crystal in the vicinity of the head dislocation in the order of 0.1–0.2°. This is enough for a detectable modification of the reflection conditions because it results in a noticeable change of the deviation from Bragg angle. For example, in the case of Fig. 7, the dislocations within the pile up are subjected to a **g**–3.2**g** diffracting condition, while the head dislocation would then be observed in the **g**–2.9**g** condition ($\omega_3 \cong 0.175°$), thus, resulting in a stronger contrast for the leading dislocation.

Another way to reproduce this effect is simply to simulate the contrast of the head dislocation in the stress field generated by the other dislocations in the pile up. This has been done assuming a pile up of four perfect dislocations distant from 30, 90 and 140 nm, respectively, mimicking the exact arrangement of Fig. 7. Again, the simulations are in good agreement with the observations, including the effect of the change of the sign of **g**.

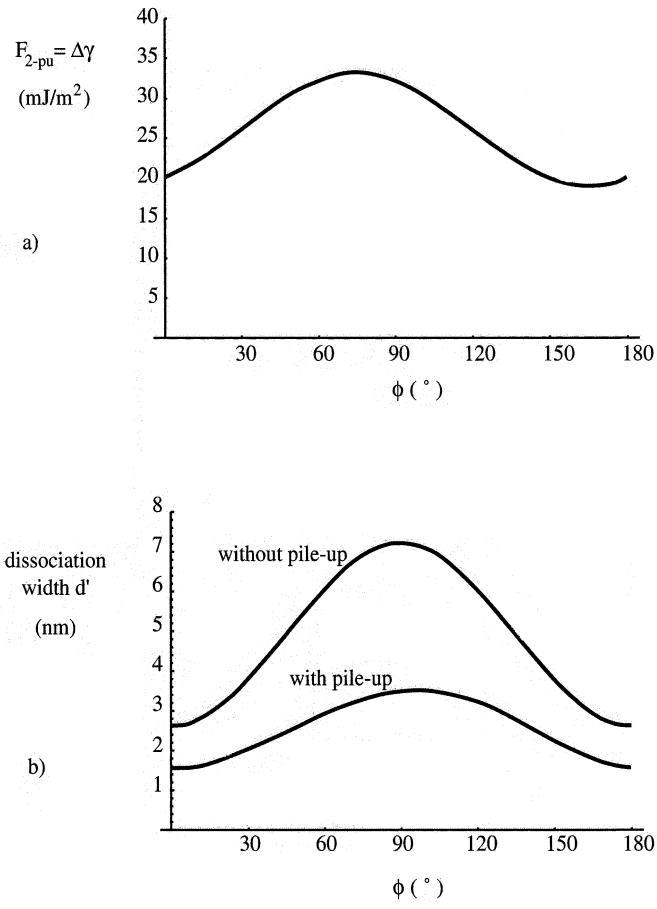

Fig. 9. (a) Force $F_{2-\mathrm{pu}} = \Delta\gamma$ experienced by the trailing partial of the leading dislocation resulting from the vicinity of the pile-up, as a function of the perfect dislocation character ϕ. The calculation includes 10 perfect dislocations and has been performed for the configuration leading to the formation of an intrinsic stacking fault. The value of ΔF for the configuration leading to an extrinsic stacking fault can be obtained by changing ϕ in $(\pi - \phi)$; (b) corresponding variation of the dissociation distance d'.

4. Discussion

Our results can be summarised as follows:

- the deformation is very localised up to 750 °C and is homogenous at 1050 °C,
- the addition of 4% of Re and Ru has no significant effect on the SFE of these model γ phases of nickel base superalloys. In both alloys, the SFEs are low and remain constant or only slightly decrease with temperature from 750 °C,
- the calculated dissociation distance of the leading dislocation of a pile up can be decreased up to 50% in response to the interaction stress created by the other dislocations of the pile up. Within the pile up, the dissociation distance is the same for all the other parallel dislocations, and is not modified by the interaction stress.

The SFE has been shown to be small, and not to vary appreciably with temperature. Furthermore, the addition of either Re or Ru does not change the stacking fault energy. Therefore, the Suzuki effect, which is proportional to the variation of the SFE with concentration $\partial\gamma_{\mathrm{SF}}/\partial c$ [21,22], plays a minor role.

On the other hand, diffuse neutron scattering experiments have clearly proved the existence of SRO, characterised by {11/20} maxima from 25 to 750 °C [11,23]. The diffuse antiphase boundary energy associated with short range order, determined from the analysis of dislocation motion under stress, decreases in temperature from 750 °C (for example is equal to 60 mJ m^{-2} at 25 °C and to 20 mJ m^{-2} at 750 °C [24]). This indicates a decrease in SRO with temperature from 750 °C, and is related to the observations that dislocations at the head of the pile up are not paired around 750 °C [25]. The transition from the heterogeneous to the homogeneous mode is correlated with the disappearance of the SRO at high temperature, not with a change of SFE. Note that the predominant influence of the diffuse antiphase boundary energy associated with SRO, compared with the stacking fault energy, on the heterogeneous-homogeneous transition has already been observed in Ni–Cr alloys and in copper solid solutions [26,27]. The friction stress induced by SRO is likely to prevent the extension of most of the dislocations despite the small value of the SFE. This is probably the reason why such a small number of extended stacking faults is observed.

Finally, we have seen that the stress in the pile up has no influence on the splitting width of the dislocations except for the leading one. Despite the effect of stress, the width of the latter remains appreciable. These conclusions agree with the fact that almost no cross-slip is observed. Besides the SRO probably contributes to inhibit cross-slip.

5. Conclusion

By using weak beam measurements and computer simulated images of dislocation dissociation widths, the evolution in temperature of the stacking fault energy of model γ phases of single crystals superalloys of the third generation containing Re or Ru was determined. The influence of alloying elements is found to be weak: the obtained values for the SFE are similar to those existing in recent industrial superalloys, for example CMSX2, AM1 or MC2 industrial superalloys. As the addition of Re and Ru have no measurable effect on the SFE, the improvement of the mechanical properties of these last generation superalloys can not be connected with the stacking fault energy.

The SFE remains quite constant ($\gamma_{SF} = 31 \pm 4$ mJ m^{-2} for Re and 28 ± 6 mJ m^{-2} for Ru) in the temperature range 25–750 °C where SRO is known to be present. Thus SRO appears to act at least at two different levels: it stabilises the SFE values when the temperature varies, then it controls, by the way of the diffuse antiphase boundary energy, the deformation micromechanisms.

The effect of the internal stress due the presence of dislocation pile ups on the dissociation was analysed. It was found to be significant for the first dislocation with a maximal decrease of the dissociation distance of 50%.

Acknowledgements

The authors are indebted to J. Crestou and A. Faccioli, CEMES, for the preparation of the TEM samples. They also thank G. Vanderschaeve for helpful discussions and for critical reading of the manuscript. This study was supported by the DRET contract no 96-2561A.

References

[1] T. Khan, in: W. Betz, R. Brunetaud, D. Coutsouradis, H. Fischmeister, T.B. Gibbons, I. Kvernes, Y. Lindblom, J.B. Marriot, D.B. Meadowcroft (Eds.), High Temperature Alloys for Gas Turbines and Other Applications, Part I, D. Reidel Publishing Company, Dordrecht, Holland, 1986, pp. 21–50.

[2] G.L. Erickson, in: R.D. Kissinger, D.J. Deye, D.L. Anton, A.D. Cetel, M.V. Nathal, T.M. Pollock, D.A. Woodford (Eds.), Superalloys 1996, The Minerals, Metals and Materials Society, Warrendale, PA, USA, 1996, pp. 35–44.

[3] W.S. Walston, K.S. O'Hara, E.W. Ross, T. Pollock, W.H. Murphy, in: R.D. Kissinger, D.J. Deye, D.L. Anton, A.D. Cetel, M.V. Nathal, T.M. Pollock, D.A. Woodford (Eds.), Superalloys 1996, The Minerals, Metals and Materials Society, Warrendale, PA, USA, 1996, pp. 27–34.

[4] P. Caron, T. Khan, in: J. Lecomte-Beckers, F. Schubert, P.J. Ennis (Eds.), Materials for Advanced Power Engineering 1998, Part II, Forschungzentrum Jülich Gmbh, Jülich, Germany, 1998, pp. 897–912.

[5] P. Caron, in: T.M. Pollock, R.D. Kissinger, R.R. Bowman, K.A. Green, M. McLean, S.L. Olson, J.J. Schirra (Eds.), Superalloys 2000, TMS, Warrendale, PA, USA, 2000, pp. 737–746.

[6] D. Blavette, P. Caron, T. Khan, Scr. Metall. 20 (1986) 1395–1400.

[7] D. Blavette, Private communication (1998).

[8] S. Duval, S. Chambreland, P. Caron, D. Blavette, Acta Metall. Mater. 42 (1994) 185–194.

[9] V.V. Rtishchev, in: D. Coutsouradis, J.H. Davidson, J. Ewald, P. Greenfield, T. Khan, M. Malik, D.B. Meadowcroft, V. Regis, R.B. Scarlin, F. Schubert, D.V. Thornton (Eds.), Materials for Advanced Power Engineering, Part I, Kluwer Academic Publishers, Dordrecht, The Netherlands, 1994, pp. 889–897.

[10] N. Clément, A. Coujou, Y. Calvayrac, F. Guillet, D. Blavette, S. Duval, Microsc. Microanal. Microstruct. 7 (1996) 65–84.

[11] R. Glas, M. Jouiad, P. Caron, N. Clément, H.O.K. Kirchner, Acta Mater. 44 (12) (1996) 4917–4926.

[12] M. Jouiad, F. Pettinari, N. Clément, A. Coujou, Phil. Mag. A79 (1999) 2591–2602.

[13] M. Benyoucef, B. Décamps, A. Coujou, N. Clément, Phil. Mag. A 71 (1995) 907–923.

[14] N. Clément, P. Coulomb, Phil Mag A 30 (1974) 663–672.

[15] E.H. Köster, A.R. Thölen, A. Howie, Phil Mag A 10 (1964) 1093–1095.

[16] D.J.H. Cockayne, J. Phys. Paris 35 (1974) C7 141–C7 148.

[17] R. Schäublin, P.A. Stadelmann, Mater. Sci. Eng. A 164 (1993) 373–378.

[18] T.M. Pollock, A.S. Argon, Acta Metall. Mater. 42 (6) (1994) 1859–1874.

[19] V. Gerold, H.P. Karnthaler, Acta Metall. Mater. 37 (1989) 2177–2183.

[20] J. Douin, PhD Thesis, University of Poitiers, France, 1987.

[21] H. Saka, Y. Kaneko, in: H. Oikawa, K. Maruyanma, S. Takeuchi, M. Yamaguchi (Eds.), Proceedings of the 10th International Conference on the Strength of Materials (ICSMA 10), Sendai, The Japan Institute of Metals, 1994, pp. 3–7.

[22] Y. Kaneko, K. Kaneko, A. Nohara, H. Saka, Phil. Mag. A 71 (2) (1995) 399–407.

[23] F. Pettinari, M. Prem, G. Krexner, P. Caron, A. Coujou, H.O.K. Kirchner, N. Clément, Acta Mater. 49 (2001) 2549–2556.

[24] F. Pettinari, PhD Thesis, University of Toulouse, France, 1999.

[25] F. Pettinari, M. Jouiad, P. Caron, H. Calderon, A. Coujou, N. Clément, Revue Française de Métallurgie CIT/Science et Génie des Matériaux (2000) 1037–1046.

[26] J. Plessing, C. Achmus, H. Neuhäuser, B. Schönfeld, G. Kostorz, Z. Metallkd. 88 (8) (1997) 630–635.

[27] K. Wolf, H.-J. Gudladt, H.A. Calderon, G. Kostorz, Acta Metall. Mater. 42 (11) (1994) 3759–3765.